*Iranian Journal of Catalysis 9(2), 2019, 133-145*

IRANIAN JOURNAL OF CATALYSIS

# Optimizing the vacuum gas oil hydrocracking process temperature in the presence of Ni-Mo/γ-$Al_2O_3$-$SiO_2$ catalyst

**Ehsan Taghizadeh Yusefabad[a], Ahmad Tavasoli[a,*], Yahya Zamani[b]**

[a]*School of Chemistry, College of Science, University of Tehran, Tehran, Iran.*
[b]*Research Institute of Petroleum Industry (RIPI), Tehran, Iran.*

Received 28 June 2018; received in revised form 20 August 2018; accepted 25 September 2018

ABSTRACT

A suitable model for predicting the product quality of vacuum gas oil (VGO) catalytic hydrocracking is developed. Data were obtained using an experimental catalytic hydrocracking reactor loaded with the Ni-Mo/$Al_2O_3$-$SiO_2$ catalyst. A set of experimental runs was conducted under various operating temperatures from 380 to 450 °C. Three distribution models were used to develop the predictive model. By the discrete lumping model, distillation curves of the cracked products (naphtha, kerosene, diesel, and gas) were obtained using the simulated distillation test. Model validation results showed that the proposed models are capable of predicting the distillation curves of the hydrocracked products accurately. Accuracy and simplicity of the developed model make it suitable to estimate the conversion and also the product distribution of hydrocracking units in refineries.

***Keywords**: VGO, Hydrocracking, Discrete lumping model.*

## 1. Introduction

The demand for the high-quality light fuels conforming to environmental standards is increased during the past several years [1,2]. Most recently explored petroleum reservoirs are also categorized as heavy oils and the conventional crude oils is depleted [1,3]. Moreover, significant sources of heavy oil fractions and residue obtained from refinery processes await new methods of recovery and upgrading [4]. An alternative hydrocracking process called hydroconversion is a new initiative to meet these requirements and convert heavy oil fractions into lighter and more useful products. Hydroconversion, which is a catalytic hydrocracking process carried out in the presence of very fine ultra-dispersed catalysts and hydrogen, produces light oils (possessing high API) with low contents of sulfur and heavy metals from the heavy oils (with low API) containing significant amounts of sulfur and heavy metals [1].

An appropriate kinetic model for hydroconversion is crucial for a proper reactor design. Results of such kinetic models can also be used for process simulation and optimization [2].

*Corresponding author.
E-mail address: tavasoli.a@ut.ac.ir (A. Tavasoli)

There are different approaches for kinetic modeling of hydrocracking of heavy oil fractions, they have been reviewed by Ancheyta et al. [2]. Kinetic modeling of hydrocracking of heavy petroleum fractions is often performed in the lumped form due to the complex nature of the feedstock containing a large number of hydrocarbons involved in a network of series and parallel reactions [2,5].

Various kinetic modeling of VGO hydrocracking reactions has been developed and studied by models such as the discrete lumping [6] and continuous lumping [7]. In the lump modeling, the mixture of the reaction is considered as the lumped pseudo-components which could be characterized by physical properties such as the ASTM boiling point, carbon numbers, molecular weight ranges, and other structural characteristics [8]. By a continuous distribution function, Astarita and Ocone [8,9] proposed lumping of nonlinear kinetics for describing VGO hydrocracking. They proposed that the kinetic behavior of the mixture followed functional-differential equations. They showed that the overall order of the reaction depends on the kinetic parameters and the initial concentration distribution, [8,10]. Ignacio Elizalde and Jorge Ancheyta studied the effect of temperature and TOS on the hydrocracking of residue Oil. They observed that the kinetic model allows to

capture the general trend of hydrocracking, and the derived model parameters undergo changes at the different TOS, confirming the fact that these parameters are a function of catalyst activity [11]. Per Julian Becker et al. described a continuous lumping model applied to hydrocracking of VGO feedstock on zeolite catalysts and compared the single events model performance with a continuous lumping model including (Paraffin, Naphthene, Aromatic) PNA families. Using the continuous lumping model, they showed that the estimation of both yield structure and PNA distribution (by standard cuts) is much better [12].

The activation energies for hydrocracking reactions of heavy oils and residue reported by different investigators [13,14] indicate substantial differences between values reported for the same reaction path. For example, the values reported by Sánchez et al. [13] indicated that the lighter products from hydrocracking would have the lower activation energy for the hydrocracking reaction. On the other hand, the sequence of activation energies reported by Loria et al. [15] and Martínez and Ancheyta [16] indicated that the lighter the products from hydrocracking would enjoy the higher activation energy for hydrocracking reactions. The activation energies reported by Hassanzadeh and Abedi [14] showed no clear pattern. The differences in the catalyst properties, feed characteristics, experimental conditions, and the algorithms used for parameters estimation might have led to these discrepancies. However, it seems that most of these investigators have only used a mathematical algorithm for kinetic parameter estimation without taking the chemistry of hydrocracking reactions into consideration.

In this work, we investigated the reaction of VGO hydrocracking at temperature of 380, 400, 420, 430, 440, and 450 ℃. VGO was provided from Tehran oil refinery. The catalyst used in this investigation is Ni-Mo/$Al_2O_3$-$SiO_2$. We prepared three discrete lumping models in different temperature ranges. The results will provide a solution to estimate VGO conversion during the hydrocracking process.

## 2. Experimental

### *2.1. Materials*

Alumina ($Al_2O_3$) granule, Silica, Ammonium heptamolybdate, and Nickle nitrate were purchased from (Sasol Company, the JSE in South Africa). The main physicochemical properties of Silica, Nickle nitrate, and Ammonium heptamolybdate sample are described in Table 1S.

Alumina ($Al_2O_3$) granule, Silica, Ammonium heptamolybdate, and Nickle nitrate were purchased from (Sasol Company, the JSE in South Africa). The main physicochemical properties of Silica, Nickle nitrate, and Ammonium heptamolybdate sample are described in Table 1S.

Physical and chemical properties of the VGO feedstock (prepared from Tehran oil refinery) are listed in Table 2S.

The pseudo-components studied in the discrete lump kinetic model and their distillation ranges are presented in Table 3S.

### *2.2. Catalyst*

#### *2.2.1. Support preparation*

$SiO_2$–$Al_2O_3$ support was obtained by homogeneous co-precipitation using sodium silicate ($Na_2Si_3O_7$, 2 M, 27% $SiO_2$/10% NaOH, Riedel de Haein) and aluminum nitrate 2 M [$Al(NO_3)_3 \cdot 9H_2O$, 2 M, 98.5%, Fermont] as precursors, and ammonium hydroxide ($NH_4OH$, 10 vol.%, 29.5% $NH_3$, Fermont) as the precipitating agent. Aqueous solutions of both precursors were mixed together slowly. Initially, silica was gelled at pH ≈ 2–3 and subsequently aluminum hydroxide was precipitated by adding $NH_4OH$ and then increasing the pH up to ≈8–9. The mixed precipitate was stirred for 1 h and finally kept overnight at 60–70 ℃ (pH ≈ 9).

The precipitate was filtered and washed with the amount of distilled water required in order to eliminate all the $Na^+$ ions. The solid was extruded (the support diameter is 1/16″) and dried at room temperature, and then at 120 ℃, and finally calcined at 550 ℃ for 4 h.

#### *2.2.2. Catalyst preparation*

Nickel–molybdenum supported catalysts were prepared by the incipient wetness co-impregnation method (pH ≈ 5.4) using aqueous solutions with the appropriate amounts of nickel nitrate and ammonium heptamolybdate to obtain 7.5 wt.% MoO3 and 2.1 wt.% NiO. The impregnated catalysts were dried in air at 120 ℃ and calcined at 450 ℃ for 4 h.

#### *2.2.3. Catalyst characterization*

The XRD pattern of the catalyst was recorded using a Bruker Advance diffractometer with Da Vinci geometry using a Ni-filtered CuKα radiation (40 kV, 30 mA) instrument. Catalysts (0.2 g) were ground in a mortar to a particle size of 38 μm. The occurrence of the respective oxidized species of the metals incorporated in wide angle analyzes was performed for all catalysts. 2θ range was scanned between 10° and 80°. By comparing the observed pattern with the diffraction pattern reported in the database PDF-4 + ICDD ($SiO_2$-00-058-0344), qualitative analysis of the observed peaks was carried out [17].

### 2.3. Reaction systems

#### 2.3.1. Testing of the catalysts in VGO hydrocracking

Hydrocracking of Vacuum Gas Oil (VGO) was conducted on a stainless steel tubular fixed-bed down-flow reactor. In this setup, the reactor is 10 mm in inner diameter and 450 mm in length. The feedstock was inserted into the reactor and it was controlled by an HPLC pump (KNAUER K-501). The mass flow controller (Brooks 5850) device was employed for injecting hydrogen into the reaction section. The pressure of the reaction system was controlled by a backpressure valve and the reaction temperature was adjusted by an electrical heater. TIC WEST 3400 was adopted for monitoring and controlling the reaction temperature.

One-gram catalyst was fed to the reactor and reduced by $H_2$ gas at pressure 150 bar and a space velocity of 200 $h^{-1}$ with constant heating rate from ambient to 453 K and maintained at this temperature for 1 h. For preparing Ni-Mo-S phases, the catalyst was sulfided by a stream of 1 wt% of dimethyl disulfide in hexane. Conditions of sulfidation are as follows: hydrogen atmosphere with an $H_2$/Oil volumetric ratio of 80 nl/L at 150 bar and a space velocity of 200 $h^{-1}$. Then, the samples were heated from 453 to 583 K with a constant heating rate of 0.5 K/min and kept at this temperature for 10 h. After the activation step, the performance of catalyst was evaluated in VGO hydrocracking. Conditions of the reaction are as follows: The injection rate of 30 $cm^3$/h and $H_2$/Oil = 175 nl/L, 150 bar, WHSV = 3 kg/ (L·h), LHSV = 4.2 $h^{-1}$. Schematic of the experimental setup is depicted in Fig. 1.

### 2.4. Model development

#### 2.4.1. Kinetic model

Modeling of hydrocracking process has evolved strikingly over the last few decades [12]. Two different lump kinetic models using a limited number of lumps (considerably less than 10) have been studied and used for the modeling of VGO hydrocracking reaction, by the discrete and continuous lumping. According to research results obtained by Barkhordari et al., priority of discrete lumping is more than the continuous lumping [8]. They have suggested that discrete lumping model is closer to the experimental value, in other words; accuracy of discrete lumping modeling is more than the continuous one. So, in this paper, the discrete lumping model of VGO hydrocracking was investigated in six different temperatures, 380, 400, 420, 430, 440, and 450.

#### 2.4.2. Discrete lumping model

In the discrete lumping model since compounds have been defined as a lump, it could be dispensed with a single reaction and conversions which happened in frontiers of lumps for describing chemical reactions and results of a lump conversion into the other. In this model, any kind of mass conversion of lump with a high molecular weight into the lighter one should be considered. Many different lumps could be considered to describe a reaction. When the number of lumpings considered for a reaction increases, results of modeling are more accurate but it should be noted that increasing lumping of model enhances the number of parameters s needed for mathematical calculations. This kinetic is used for obtaining kinetic equations needed for resulting complex reactions. Separate lumping used for catalytic hydrocracking of VGO is classified based on the difference between boiling points of compounds; while for searching higher molecular reactions such as bitumen, coal and oil residuals, lumps have been classified based on certain particles and molecular masses. In this investigation, different routes of lumping models are tested and correctitude of them was measured. In all of these routes, five lumps, feed (VGO), diesel, kerosene, naphtha and LPG, have been used. All of mentioned reactions have been supposed irreversible and first order reactions.

#### 2.4.3. Description of the kinetic model and the procedure for the parameter estimation

Various discrete lump models were proposed for explaining the reaction kinetic of VGO hydrocracking [18]. Apart from VGO, diesel could be cracked into other lighter cuts in higher temperatures (Fig. 2b) and in very high temperatures all of the liquids which are produced from VGO hydrocracking can be converted into gas (Fig. 2c). Rates of VGO hydrocracking are assumed to follow first-order kinetics [9].

In catalytic processes, the diffusion agent affects the process kinetics. Since solving kinetic equations related to diffusion is very difficult and time-consuming, this factor is considered as one of the constituents of kinetics constants. In other words, the kinetic constant k depends on the amount of diffusion. Kinetic equations are obtained by solving the first-order integral equations of VGO hydrocracking. Kinetic equations of the VGO following the model (2a) are listed in Table 1.

Assuming that the ratio of the mass ratio of feed at the beginning of the reaction is equal to one and that of D, K, N, and G is zero, the equations in Table 1 are listed (Table 2).

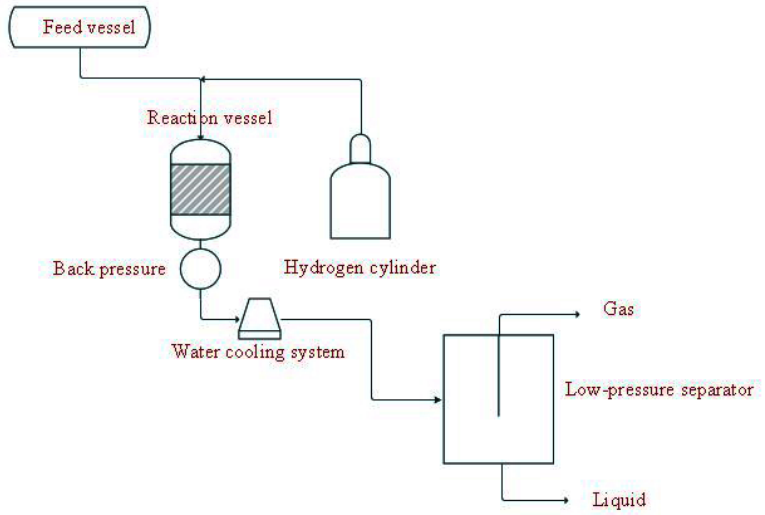


**Fig. 1.** The schematic of the experimental setup.

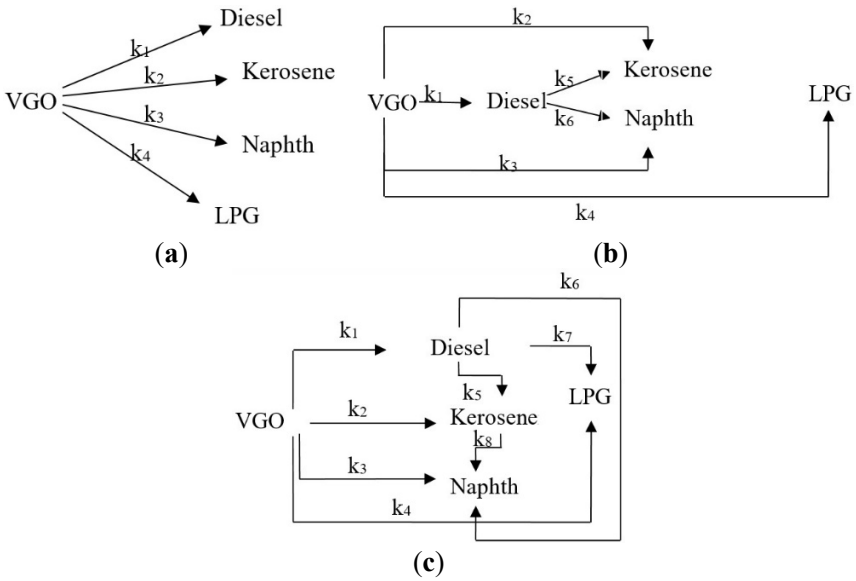


**Fig. 2.** Models proposed for hydrocracking process in different temperatures.

**Table 1.** Kinetic differential equations of the VGO hydrocracking when the VGO hydrocracking followed model (2a) [8].

| Number | Kinetic differential equation |
|---|---|
| (**1**) | $\frac{dF}{dt} = -(k_1 + k_2 + k_3 + k_4)F$ |
| (**2**) | $\frac{dD}{dt} = k_1 F$ |
| (**3**) | $\frac{dK}{dt} = k_2 F$ |
| (**4**) | $\frac{dN}{dt} = k_3 F$ |
| (**5**) | $\frac{dG}{dt} = k_4 F$ |

F is the amount of initial feed (VGO) in terms of mass ratio, D is the amount of the produced diesel in terms of mass ratio, K is the amount of the produced kerosene in terms of mass ratio, N is the amount of the produced naphtha in terms of mass ratio, G is the amount of the produced gas in terms of mass ratio and $k_1$, $k_2$, $k_3$ and $k_4$ is in terms of $lit^{-1}\ s^{-1}$.

**Table 2.** Kinetic equations of the VGO hydrocracking when the VGO hydrocracking followed model (2a).

| Number | Kinetic equation |
|---|---|
| (**6**) | $F = e^{-(k_1+k_2+k_3+k_4)t}$ |
| (**7**) | $D=\frac{-k_1}{(k_1+k_2+k_3+k_4)}e^{-(k_1+k_2+k_3+k_4)t}+\frac{k_1}{(k_1+k_2+k_3+k_4)}$ |
| (**8**) | $K=\frac{-k_2}{(k_1+k_2+k_3+k_4)}e^{-(k_1+k_2+k_3+k_4)t}+\frac{k_2}{(k_1+k_2+k_3+k_4)}$ |
| (**9**) | $N=\frac{-k_3}{(k_1+k_2+k_3+k_4)}e^{-(k_1+k_2+k_3+k_4)t}+\frac{k_3}{(k_1+k_2+k_3+k_4)}$ |
| (**10**) | $G=\frac{-k_4}{(k_1+k_2+k_3+k_4)}e^{-(k_1+k_2+k_3+k_4)t}+\frac{k_4}{(k_1+k_2+k_3+k_4)}$ |

To solve kinetic equations of the model 2b, the model could be written as follows:

$$F + H_2 \xrightarrow{K_1} V_1D + V_2K + V_3N + V_4G \quad (\mathbf{11})$$

$$D \xrightarrow{K_2} V_5K + V_6N \quad (\mathbf{12})$$

In equations 11 and 12, the constants $K_1$, $K_2$, $V_1$, $V_2$, $V_3$, $V_4$, $V_5$ and $V_6$ are the kinetic constants. According to equations 11 and 12, the model 2b and kinetic constants, the following relations exist between constants:

$$K_1V_1 = k_1 \quad (\mathbf{13})$$

$$K_1V_2 = k_2 \quad (\mathbf{14})$$

$$K_1V_3 = k_3 \quad (\mathbf{15})$$

$$K_1V_4 = k_4 \quad (\mathbf{16})$$

$$K_2V_5 = k_5 \quad (\mathbf{17})$$

$$K_2V_6 = k_6 \quad (\mathbf{18})$$

Kinetic differential equations of the VGO hydrocracking when the reaction followed of model 2b are listed in Table 3.

Assuming that the ratio of the mass ratio of feed at the beginning of the reaction is equal to one and that of D, K, N, and G is zero, the equations in Table 6 are listed as follows (Table 4).

**Table 3.** Kinetic differential equations of the VGO hydrocracking when the VGO hydrocracking followed model (2b).

| Number | Kinetic equation |
|---|---|
| (**19**) | $\frac{dF}{dt} = -K_1\left(V_1+V_2+V_3+V_4\right)F$ |
| (**20**) | $\boxed{\frac{dG}{dt} = V_4K_1F}$ |
| (**21**) | $\boxed{\frac{dN}{dt} = V_3K_1e^{-K_1(V_1+V_2+V_3+V_4)t} + V_6K_2\left(\frac{K_1V_1}{K_2\left(V_5+V_6\right)-K_1\left(V_1+V_2+V_3+V_4\right)}\left(e^{-K_1(V_1+V_2+V_3+V_4)t}-e^{-K_2(V_5+V_6)t}\right)\right)}$ |
| (**22**) | $\boxed{\frac{dD}{dt} = K_1V_1F - K_2\left(V_5+V_6\right)D}$ |
| (**23**) | $\boxed{\frac{dK}{dt} = V_2K_1e^{-K_1(V_1+V_2+V_3+V_4)t} + V_5K_2\left(\frac{K_1V_1}{K_2\left(V_5+V_6\right)-K_1\left(V_1+V_2+V_3+V_4\right)}\left(e^{-K_1(V_1+V_2+V_3+V_4)t}-e^{-K_2(V_5+V_6)t}\right)\right)}$ |

F is the amount of initial feed (VGO) in terms of mass ratio, D is the amount of the produced diesel in terms of mass ratio, K is the amount of the produced kerosene in terms of mass ratio, N is the amount of the produced naphtha in terms of mass ratio, G is the amount of the produced gas in terms of mass ratio, $V_1$, $V_2$, $V_3$, $V_4$, $V_5$ and $V_6$ are in terms of $lit^{-1}\ s^{-1}$ and $K_1$, $K_2$ are constant numbers.

**Table 4.** Kinetic equations of the VGO hydrocracking when the VGO hydrocracking followed model (2b).

| Number | Kinetic equation |
|---|---|
| (**24**) | $\ln(F) = -K_1(V_1+V_2+V_3+V_4)t$ |
| (**25**) | $G = \frac{-V_4}{(V_1+V_2+V_3+V_4)} e^{-K_1(V_1+V_2+V_3+V_4)t} + \frac{V_4}{(V_1+V_2+V_3+V_4)}$ |
| (**26**) | $N = \frac{-V_3}{(V_1+V_2+V_3+V_4)} e^{-K_1(V_1+V_2+V_3+V_4)t} + \frac{K_1K_2V_1V_6}{(K_2(V_5+V_6)-(K_1V_1+K_1V_2+K_1V_3+K_1V_4))}\left(\frac{e^{-K_2(V_5+V_6)t}}{K_2(V_5+V_6)} - \frac{e^{-K_1(V_1+V_2+V_3+V_4)t}}{K_1(V_1+V_2+V_3+V_4)}\right) + \left(\frac{((V_1V_6)+V_3(V_5+V_6))}{((V_1+V_2+V_3+V_4)(V_5+V_6))}\right)$ |
| (**27**) | $D = \frac{K_1V_1}{K_2(V_5+V_6)-K_1(V_1+V_2+V_3+V_4)}\left(e^{-K_1(V_1+V_2+V_3+V_4)t} - e^{-K_2(V_5+V_6)t}\right)$ |
| (**28**) | $K = \frac{-V_2}{(V_1+V_2+V_3+V_4)} e^{-K_1(V_1+V_2+V_3+V_4)t} + \left(\frac{K_1K_2V_1V_5}{(K_2(V_5+V_6)-K_1(V_1+V_2+V_3+V_4))}\right)\left(\frac{e^{-K_2(V_5+V_6)t}}{K_2(V_5+V_6)} - \frac{e^{-K_1(V_1+V_2+V_3+V_4)t}}{K_1(V_1+V_2+V_3+V_4)}\right) + \left(\frac{(V_1V_5+V_2(V_5+V_6))}{((V_1+V_2+V_3+V_4)(V_5+V_6))}\right)$ |

To solve kinetic equations of the model (2c), the model could be written as follows:

$$feed \xrightarrow{K_1} V_1 Diesel + V_2 Kerosene + V_3 Naphtha + V_4 LPG \quad (29)$$

$$Diesel \xrightarrow{K_2} V_5 Kerosene + V_6 Naphtha + V_7 LPG \quad (30)$$

$$Kerosene \xrightarrow{K_3} V_8 Naphtha \quad (31)$$

In equation (29-31), the constants, $K_1$, $K_2$, $K_3$, $V_1$, $V_2$, $V_3$, $V_4$, $V_5$, $V_6$, $V_7$ and $V_8$ are the kinetic constants. According to the equation (29-31), the model (2c) and kinetic constants, the following equivalence relations exist between constants:

$$K_1V_1 = k_1 \quad (32)$$

$$K_1V_2 = k_2 \quad (33)$$

$$K_1V_3 = k_3 \quad (34)$$

$$K_1V_4 = k_4 \quad (35)$$

$$K_2V_5 = k_5 \quad (36)$$

$$K_2V_6 = k_6 \quad (37)$$

$$K_2V_7 = k_7 \quad (38)$$

$$K_3V_8 = k_8 \quad (39)$$

Kinetic differential equations of the VGO hydrocracking when the reaction followed model (2c) are listed in Table 5.

Assuming that the ratio of the mass ratio of feed at the beginning of the reaction is equal to one and that of D, K, N, and G is zero, the equations in Table 5 are listed as follows (Table 6).

**Table 5.** Kinetic differential equations of the VGO hydrocracking when the VGO hydrocracking followed of model (2c).

| Number | Kinetic equation |
|---|---|
| (**40**) | $\frac{dF}{dt} = -K_1\left(V_1+V_2+V_3+V_4\right)F$ |
| (**41**) | $\frac{dD}{dt} = K_1V_1F - K_2\left(V_5+V_6+V_7\right)D$ |
| (**42**) | $\frac{dK}{dt} = V_2K_1F - K_3\left(V_8\right)K$ |
| (**43**) | $\frac{dN}{dt} = K_1V_3F + K_2V_6D + K_3V_8K = K_1V_3e^{\left(-K_1(V_1+V_2+V_3+V_4)t\right)} + K_2V_6\left(\frac{K_1V_1}{K_2\left(V_5+V_6+V_7\right)-K_1\left(V_1+V_2+V_3+V_4\right)}\left(e^{\left(-K_1(V_1+V_2+V_3+V_4)t\right)} - e^{\left(-K_2(V_5+V_6+V_7)t\right)}\right)\right) + K_3V_8\left(\frac{V_2K_1}{K_3\left(V_8\right)-K_1\left(V_1+V_2+V_3+V_4\right)}\left(e^{\left(-K_1(V_1+V_2+V_3+V_4)t\right)} - e^{\left(-K_3(V_8)t\right)}\right)\right)$ |
| (**44**) | $\frac{dG}{dt} = K_1V_4F + K_2V_7D = K_1V_4e^{-K_1(V_1+V_2+V_3+V_4)t} + \frac{K_2V_7K_1V_1}{K_2\left(V_5+V_6+V_7\right)-K_1\left(V_1+V_2+V_3+V_4\right)}\left(e^{-K_1(V_1+V_2+V_3+V_4)t} - e^{-K_2(V_5+V_6+V_7)t}\right)$ |

F is the amount of initial feed (VGO) in terms of mass ratio, D is the amount of the produced diesel in terms of mass ratio, K is the amount of the produced kerosene in terms of mass ratio, N is the amount of the produced naphtha in terms of mass ratio, G is the amount of the produced gas in terms of mass ratio, $V_1$, $V_2$, $V_3$, $V_4$, $V_5$, $V_6$, $V_7$ and $V_8$ are in terms of $lit^{-1}\ s^{-1}$ and $K_1$, $K_2$, $K_3$ are constant numbers.

**Table 6.** Kinetic equations of the VGO hydrocracking when the VGO hydrocracking followed model (2c).

| Number | Kinetic equation |
|---|---|
| (**45**) | $F = e^{-K_1(V_1+V_2+V_3+V_4)t}$ |
| (**46**) | $D = \left(\frac{K_1V_1}{\left(K_2\left(V_5+V_6+V_7\right)-K_1\left(V_1+V_2+V_3+V_4\right)\right)}\right)\left(e^{-K_1(V_1+V_2+V_3+V_4)t} - e^{-K_2(V_5+V_6+V_7)t}\right)$ |
| (**47**) | $K = \left(\frac{V_2K_1}{\left(K_3\left(V_8\right)-K_1\left(V_1+V_2+V_3+V_4\right)\right)}\right)\left(e^{-K_1(V_1+V_2+V_3+V_4)t} - e^{-K_3(V_8)t}\right)$ |
| (**48**) | $N = \left(\frac{-V_3}{\left(V_1+V_2+V_3+V_4\right)}\right)e^{\left(-K_1(V_1+V_2+V_3+V_4)t\right)} + \left(\frac{K_1K_2V_1V_6}{\left(K_2\left(V_5+V_6+V_7\right)-K_1\left(V_1+V_2+V_3+V_4\right)\right)}\right)\left(\frac{e^{\left(-K_2(V_5+V_6+V_7)t\right)}}{\left(K_2\left(V_5+V_6+V_7\right)\right)} - \frac{e^{\left(-K_1(V_1+V_2+V_3+V_4)t\right)}}{\left(K_1\left(V_1+V_2+V_3+V_4\right)\right)}\right) + \left(\frac{K_1K_3V_2V_8}{\left(K_3\left(V_8\right)-K_1\left(V_1+V_2+V_3+V_4\right)\right)}\right)\left(\frac{e^{\left(-K_3(V_8)t\right)}}{\left(K_3\left(V_8\right)\right)} - \frac{e^{\left(-K_1(V_1+V_2+V_3+V_4)t\right)}}{\left(K_1\left(V_1+V_2+V_3+V_4\right)\right)}\right) + \left(\frac{V_3}{\left(V_1+V_2+V_3+V_4\right)}\right) - \left(\frac{K_1K_2V_1V_6}{\left(K_2\left(V_5+V_6+V_7\right)-K_1\left(V_1+V_2+V_3+V_4\right)\right)}\right)\left(\frac{1}{\left(K_2\left(V_5+V_6+V_7\right)\right)} - \frac{1}{\left(K_1\left(V_1+V_2+V_3+V_4\right)\right)}\right) - \left(\frac{K_1K_3V_2V_8}{\left(K_3\left(V_8\right)-K_1\left(V_1+V_2+V_3+V_4\right)\right)}\right)\left(\frac{1}{\left(K_3\left(V_8\right)\right)} - \frac{1}{\left(K_1\left(V_1+V_2+V_3+V_4\right)\right)}\right)$ |

**Table 6.** (*Continued*)

| | |
|---|---|
| (**49**) | $G=\left(\left(\frac{-V_4}{(V_1+V_2+V_3+V_4)}\right)e^{\left(-K_1(V_1+V_2+V_3+V_4)t\right)}\right)+\left(\frac{K_1K_2V_1V_7}{\left(\left(K_2(V_5+V_6+V_7)\right)-\left(K_1(V_1+V_2+V_3+V_4)\right)\right)}\right)\left(\left(\frac{e^{\left(-K_2(V_5+V_6+V_7)t\right)}}{\left(K_2(V_5+V_6+V_7)\right)}\right)-\left(\frac{e^{\left(-K_1(V_1+V_2+V_3+V_4)t\right)}}{\left(K_1(V_1+V_2+V_3+V_4)\right)}\right)\right)+\left(\frac{V_4}{(V_1+V_2+V_3+V_4)}\right)-\left(\frac{K_2V_7K_1V_1}{\left(K_2(V_5+V_6+V_7)\right)-\left(K_1(V_1+V_2+V_3+V_4)\right)}\right)\left(\left(\frac{1}{\left(K_2(V_5+V_6+V_7)\right)}\right)-\left(\frac{1}{\left(K_1(V_1+V_2+V_3+V_4)\right)}\right)\right)$ |

In above equations, the kinetic rate constants, $k_1$, $k_2$, $k_3$, $k_4$, $k_5$, $k_6$, $k_7$, and $k_8$ were calculated by fitting the experimental data and the equations in Levenberg-Marquart algorithm.

*2.4.4. Catalyst deactivation*

Catalyst deactivation could affect the activity of catalyst and therefore the kinetic discrete lumping model. To diminish this effect, experimental data were obtained at first two-hours after placing the catalyst in the reactor. An exponential function is used to show the activation coefficient of catalyst on stream with the time:

$$\varphi = Exp\left(-k_d t_e\right) \quad (\mathbf{50})$$

In the above equation, ($k_d$) could be predicted using experimental data obtaining during a long term operation [8].

## 3. Results and Discussion

*3.1. Catalyst characterization*

The XRD pattern of Ni-Mo/$Al_2O_3$-$SiO_2$ catalyst is illustrated in Fig. 3. The γ-alumina, $Al_2O_3$-$SiO_2$, $MoO_3$, NiO and phases are observed in the XRD patterns. In this study, three diffraction peaks that appeared at 2θ of 37, 46, and 67° (A) (Reference code: 00-001-1243) [19] for all catalysts are assigned to γ-$Al_2O_3$ appeared in all catalysts prepared. Several diffraction peaks for $Al_2O_3$-$SiO_2$ appeared at 2θ values of 17, 26, 33, 37, 39, 45, and 49° (S) (Reference code: 00-002-0469). Diffraction peaks for $MoO_3$ appeared at 2θ values of 23, 27, and 45° (M) (Reference code: 00-005-0506) [19]. The observation reflects that $MoO_3$ is well dispersed on the catalyst surface. Diffraction peak for NiO appeared at the 2θ value of 37° (N) (Reference code: 00-004-0835).

*3.2. Catalytic Results at different temperature*

Based on data obtained from the reactor in various temperature ranges, three kinetic models of the hydrocracking process of VGO were demonstrated. The parameters of the kinetic model of discrete lumping were estimated using the experimental data in different space times. Twelve data at six space times (0.33, 0.4, 0.5, 0.67, 1, and 2 h) were used at a constant operating temperature to estimate the kinetic parameters. The data were examined at various temperatures of 380, 400, 420, 430, 440, and 450 °C to predict the main kinetic parameters and models at different temperatures. The results of 24 test runs at different space times and temperatures between 380-430 °C are shown in Table 7.

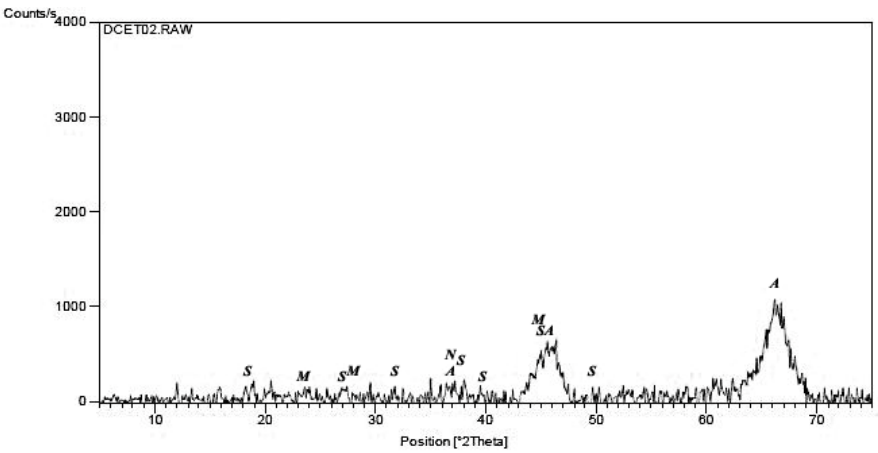


**Fig. 3.** XRD pattern of the Ni-Mo /$Al_2O_3$-$SiO_2$ catalyst, (A: $Al_2O_3$, S: $SiO_2$, M: $MoO_3$ , N: NiO).

**Table 7.** Experimental yields of each lump component at 24 test runs.

| Space time (h) | Temperature(°C) | Gas (%wt.) | Naphtha (%wt.) | Kerosene (%wt.) | Diesel (%wt.) |
|---|---|---|---|---|---|
| 0 | 380 | 0 | 0 | 0 | 0 |
| 0.33 | 380 | 1.01 | 1.27 | 3.17 | 3.60 |
| 0.4 | 380 | 1.19 | 1.50 | 3.77 | 4.45 |
| 0.5 | 380 | 1.47 | 1.81 | 4.59 | 5.28 |
| 0.67 | 380 | 1.86 | 2.29 | 6.10 | 6.98 |
| 1 | 380 | 2.66 | 3.16 | 8.75 | 10.12 |
| 2 | 380 | 4.54 | 5.34 | 15.40 | 17.73 |
| 0 | 400 | 0 | 0 | 0 | 0 |
| 0.33 | 400 | 1.85 | 2.38 | 4.80 | 5.90 |
| 0.4 | 400 | 2.17 | 2.81 | 5.89 | 7.04 |
| 0.5 | 400 | 2.46 | 3.42 | 7.03 | 8.61 |
| 0.67 | 400 | 3.34 | 4.29 | 9.22 | 11.10 |
| 1 | 400 | 4.39 | 6.18 | 12.96 | 15.46 |
| 2 | 400 | 6.97 | 8.89 | 20.85 | 25.10 |
| 0 | 420 | 0 | 0 | 0 | 0 |
| 0.33 | 420 | 3.07 | 4.44 | 6.99 | 7.68 |
| 0.4 | 420 | 3.66 | 5.25 | 7.76 | 9.18 |
| 0.5 | 420 | 4.14 | 6.46 | 9.68 | 10.93 |
| 0.67 | 420 | 5.42 | 8.04 | 11.99 | 13.96 |
| 1 | 420 | 7.24 | 11.16 | 16.56 | 18.69 |
| 2 | 420 | 10.72 | 15.91 | 24.13 | 27.52 |
| 0 | 430 | 0 | 0 | 0 | 0 |
| 0.33 | 430 | 4.81 | 6.15 | 7.26 | 8.90 |
| 0.4 | 430 | 5.55 | 7.15 | 8.35 | 10.55 |
| 0.5 | 430 | 6.01 | 8.89 | 10.31 | 12.51 |
| 0.67 | 430 | 7.61 | 11.43 | 12.63 | 15.93 |
| 1 | 430 | 9.72 | 14.99 | 16.62 | 20.62 |
| 2 | 430 | 13.65 | 20.55 | 22.84 | 28.46 |

The cumulative yield of the lump components, at each run, has been used in the discrete lump kinetic model to predict the kinetic parameters. The kinetic parameters are optimized by Levenberg-Marquardt algorithm at every temperature and listed in Table 8.

Arrhenius kinetic constants of the discrete lumping model are listed in Table 9.

The variations of naphtha, kerosene, diesel and gas between 380-430 °C are shown in Fig. 4.

**Table 8.** Optimized kinetic parameters of discrete model.

| Temp. (°C) | $k_1$ ($lit^{-1}$ $s^{-1}$) | $k_2$ ($lit^{-1}$ $s^{-1}$) | $k_3$ ($lit^{-1}$ $s^{-1}$) | $k_4$ ($lit^{-1}$ $s^{-1}$) |
|---|---|---|---|---|
| 380 | 0.1157 | 0.1004 | 0.0360 | 0.0302 |
| 400 | 0.1955 | 0.1625 | 0.0730 | 0.0556 |
| 420 | 0.2661 | 0.2333 | 0.1549 | 0.1033 |
| 430 | 0.3197 | 0.2569 | 0.2293 | 0.1543 |

**Table 9.** Arrhenius kinetic constants of the discrete lump model.

| I= Lump No. | Ln(A) | Ei/R (°K) |
|---|---|---|
| 1 | 11.892 | 9150.8 |
| 2 | 11.142 | 8755.8 |
| 3 | 22.647 | 16980 |
| 4 | 19.078 | 14765 |

According to Fig. 4, when the temperature increases, hydrocracking conversion and selectivity of naphtha and gas increase [20], but those of diesel and kerosene decrease. This subject could be the increase of temperature and light products , in other words, the feedstock conversion into distillate is thermally controlled [21]. Data of VGO hydrocracking process at 440º C are listed in Table 10. The variations of naphtha, kerosene, diesel and gas at 440 ℃ are shown in Fig. 5.

Optimized kinetic parameters of the discrete model are listed at Table 11.

It was observed that at 450 ℃, VGO hydrocracking followed the model presented in Fig. 6. Experimental yields of each lump component at 12 test runs in temperature of 450 ℃ are listed at Table 12.

Optimized kinetic parameters of the discrete model are listed in table 13.

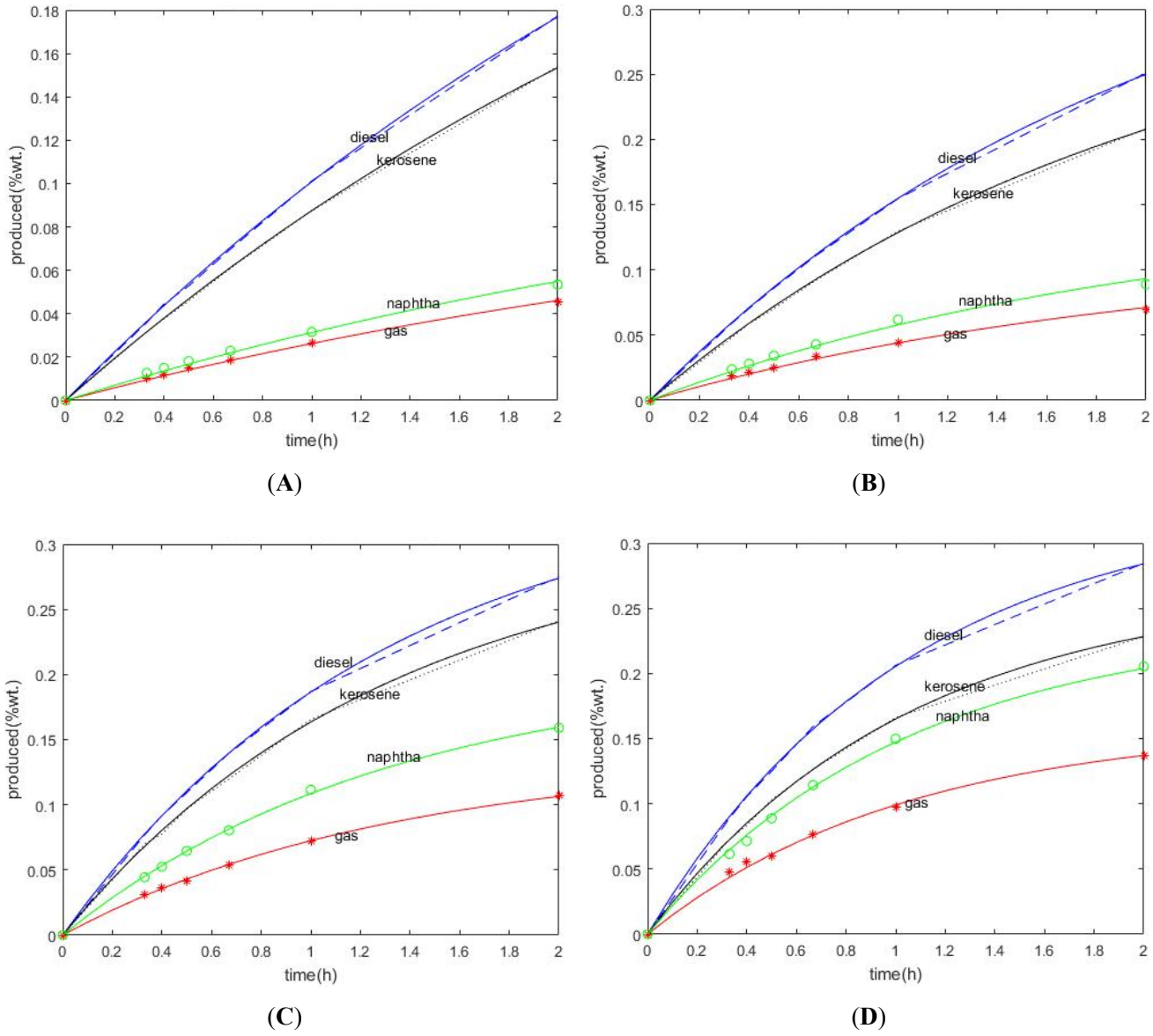


**Fig. 4.** Products of VGO hydrocracking in 380 ℃ (A), 400 ℃ (B), 420 ℃ (C), 430 ℃ (D).

**Table 10.** Experimental yields of each lump component at 12 test runs in 440 ℃.

| Space time (h) | Gas (%wt.) | Naphtha (%wt.) | Kerosene (%wt.) | Diesel (%wt.) |
|---|---|---|---|---|
| 0 | 0 | 0 | 0 | 0 |
| 0.33 | 5.61 | 8.29 | 8.10 | 11.85 |
| 0.4 | 6.75 | 9.81 | 8.09 | 13.30 |
| 0.5 | 7.84 | 12.19 | 11.18 | 15.11 |
| 0.67 | 10.21 | 15.05 | 14.23 | 17.89 |
| 1 | 12.94 | 23.37 | 18.10 | 19.18 |
| 2 | 16.47 | 35.72 | 27.19 | 14.08 |

**Table 11.** Optimized kinetic parameters of the discrete model.

| Temp. (℃) | $k_1$ (lit$^{-1}$ s$^{-1}$) | $k_2$ (lit$^{-1}$ s$^{-1}$) | $k_3$ (lit$^{-1}$ s$^{-1}$) | $k_4$ (lit$^{-1}$ s$^{-1}$) | $k_5$ (lit$^{-1}$ s$^{-1}$) | $k_6$ (lit$^{-1}$ s$^{-1}$) |
|---|---|---|---|---|---|---|
| 440 | 0.5169 | 0.2665 | 0.2653 | 0.2222 | 0.2430 | 0.5375 |

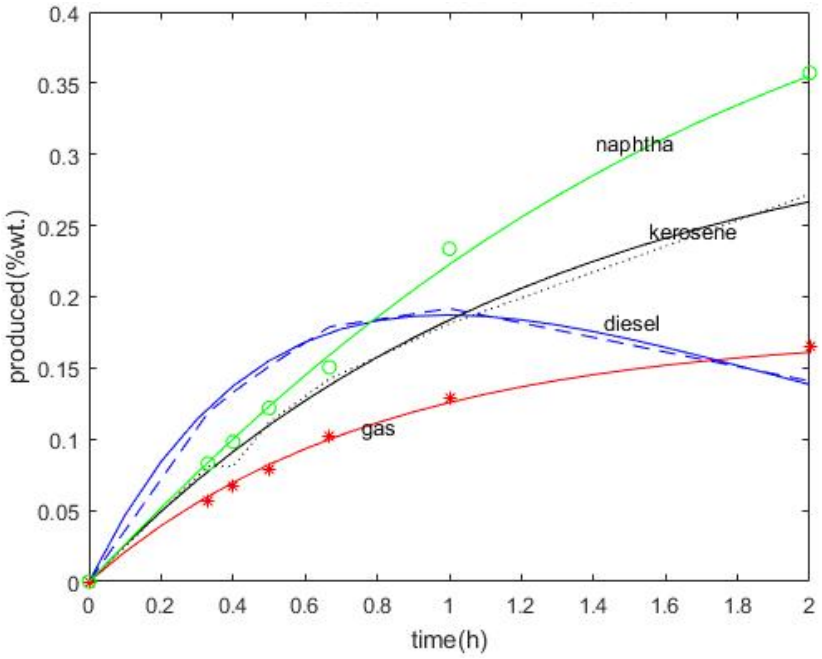


**Fig. 5.** Products of VGO hydrocracking in 440 ℃.

**Table 12.** Experimental yields of each lump component at 12 test runs in 450 ℃.

| Time (h) | Gas (%wt.) | Naphtha (%wt.) | Kerosene (%wt.) | Diesel (%wt.) |
|---|---|---|---|---|
| 0 | 0 | 0 | 0 | 0 |
| 0.33 | 5.96 | 12.67 | 13.97 | 16.06 |
| 0.4 | 7.03 | 14.87 | 15.76 | 17.31 |
| 0.5 | 8.43 | 17.89 | 16.96 | 18.88 |
| 0.67 | 10.12 | 23.86 | 18.15 | 20.97 |
| 1 | 13.52 | 34.65 | 17.62 | 20.89 |
| 2 | 21.76 | 50.69 | 10.50 | 13.49 |

**Table 13.** Optimized kinetic parameters of the discrete model.

| Temp. (°C) | $k_1$ (lit$^{-1}$ s$^{-1}$) | $k_2$ (lit$^{-1}$ s$^{-1}$) | $k_3$ (lit$^{-1}$ s$^{-1}$) | $k_4$ (lit$^{-1}$ s$^{-1}$) | $k_5$ (lit$^{-1}$ s$^{-1}$) | $k_6$ (lit$^{-1}$ s$^{-1}$) | $k_7$ (lit$^{-1}$ s$^{-1}$) | $k_8$ (lit$^{-1}$ s$^{-1}$) |
|---|---|---|---|---|---|---|---|---|
| 450 | 0.7348 | 0.6778 | 0.4032 | 0.1893 | 0.0506 | 0.2516 | 0.3623 | 0.8066 |

According to Fig. 5 and 6, at 440 °C, diesel during VGO hydrocracking increased at first and then decreased. At 450 °C and higher, kerosene could also follow these variations. This subject proved the fact that diesel and kerosene could be converted into other products (lighter pseudo-component) at 440 °C and higher. In this investigation, according to first order kinetic equations of VGO hydrocracking [8] and data obtained in the experimental setup and these equations solved by the Levenberg-Marquardt algorithm, it is clear that diesel converted into the kerosene and naphtha in 440 °C. Also, at 450 °C diesel is converted into the gas, kerosene and naphtha and then kerosene is converted into naphtha. These results suggested that amount of dry gas and naphtha could be increased when temperature increases [22], and that the conversion of the feedstock to distillate is thermally controlled [21]. Comparing the experimental and calculated data could confirm the mentioned models. It is observed that the concentration of overcracking products (LPG and dry gases) is very low between 380-430 °C. The main products are medium distillates and naphtha, and also diesel. The increase in temperature, leading to the decrease in the concentration of medium distillates and diesel enhances the formation of dry gases, LPG, and naphtha. Although the hydrogenation step (exothermic) is controlled by the thermodynamic equilibrium, the cracking step (endothermic) is enhanced by temperature.

## 4. Conclusions

Three five-lump kinetic models including 4, 5, and 6 reaction pathways were initially proposed to investigate the kinetics of VGO hydrocracking. Experimental data were obtained from an experimental-scale reactor over the Ni-Mo/$Al_2O_3$-$SiO_2$ catalyst in temperatures range of 380 to 450 °C and were used to evaluate the proposed kinetic model. Then, kinetic constants of VGO hydrocracking are calculated using Levenberg-Marquardt algorithm and changing procedures of naphtha, LPG, kerosene, and diesel produced during the VGO hydrocracking were formulated in various temperatures. Because of changes of catalyst activity along with the time and temperature, the discrete lumping modeling of VGO hydrocracking could be changed. Based on calculations, it was understood that as the temperature is increased, conversion of VGO hydrocracking and selectivity of naphtha and gas increase but those of diesel and kerosene decrease. In other words, these results proved that the conversion of the VGO to distillate is thermally controlled during the hydrocracking process.

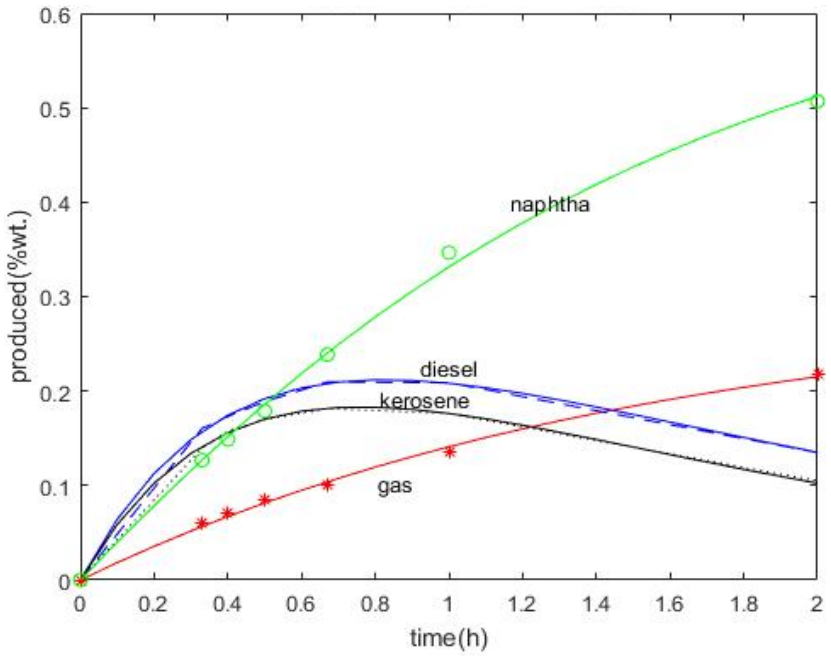


**Fig. 6.** Products of VGO hydrocracking at 450 °C.

## References


[1] T.C. Ho, Modeling of Reaction Kinetics for Petroleum Fractions, In C.S. Hsu, P.R. Robinson (Eds.), Practical Advances in Petroleum Processing, Springer, New York, 2006.

[2] J. Ancheyta, S. Sánchez, and M.A. Rodríguez, Catal. Today 109 (2005) 76–92.

[3] J. Thompson, The Synthesis and Evaluation of Molybdenum-Based Ultra-Dispersed Hydroprocessing Catalysts. M.Sc. Thesis, University of Calgary, Alberta, 2008.

[4] M.S. Rana, V. Sámano, J. Ancheyta, and J.A.I. Diaz, Fuel 86 (2007) 1216–1231.

[5] P.M. Rahimi, T. Gentzis, The Chemistry of Bitumen and Heavy Oil Processing, In C.S. Hsu, P.R. Robinson (Eds.), Practical Advances in Petroleum Processing, Springer, New York, 2006.

[6] B.E. Stangeland, Ind. Eng. Chem. Process Des. Dev. 13 (1974) 71–76.

[7] C.S. Laxminarasimhan, R.P. Verma, P.A. Ramachandran, AIChE J. 42 (1996) 2645–2653.

[8] A. Barkhordari, S. Fatemi, M. Daneshpayeh, H. Zamani, Int. J. Chem. React. Eng. 8 (2010) A81.

[9] G. Astarita, R. Ocone, AIChE J. 34 (1988)1299–1309.

[10] G. Astarita, AIChE J. 35 (1989) 529–532.

[11] I. Elizalde, J. Ancheyta, Fuel Process. Technol. 123 (2014) 114–121.

[12] P.J. Becker, N. Serrand, B. Celse, D. Guillaume, H. Dulot, Fuel 165 (2016) 306–315.

[13] S. Sánchez, M.A. Rodríguez, J. Ancheyta, Ind. Eng. Chem. Res. 44 (2005) 9409–9413.

[14] H. Hassanzadeh J. Abedi, Fuel 89 (2010) 2822–2828.

[15] H. Loria, G. Trujillo-Ferrer, C. Sosa-Stull, P. Pereira-Almao, Energy Fuels 25 (2011) 1364–1372.

[16] J. Martínez, J. Ancheyta, Fuel 100 (2012) 193–199.

[17] J.R. Restrepo-Garcia, V.G. Baldovino-Medrano, S.A. Giraldo, Appl. Catal. A 510 (2016) 98–109.

[18] J.W. Ward, Fuel Process. Technol. 35 (1993) 55–85.

[19] P.Y. Looi, A.R. Mohamed, C.T. Tye, Chem. Eng. J. 181 (2012) 717–724.

[20] A. Gutiérrez, J.M. Arandes, P. Castaño, M. Olazar, A. Barona, J. Bilbao, Chem. Eng. Technol. 35 (2012) 653–660.

[21] N. Panariti, A. Del Bianco, G. Del Piero, M. Marchionna, P. Carniti, Appl. Catal. A 204 (2000) 215–222.

[22] J. Mosio-Mosiewski, I. Morawski, Appl. Catal. A 283 (2005) 147–155.